

Mapping Embankment Dam Geomorphology Using Unmanned Aerial Vehicles (UAVs): A Case Study of Bukit Kwong Dam, Kelantan, Malaysia.

Nasuha Ishak^{1,*}, and Wani Sofia Udin^{1,2}

¹ Faculty of Earth Science, Universiti Malaysia Kelantan (Jeli Campus), 17600 Jeli, Kelantan, Malaysia

² Tropical GeoResource & Hazards Research Group, Faculty of Earth Science, Universiti Malaysia Kelantan (Jeli Campus), 17600 Jeli, Kelantan, Malaysia

Abstract. Dam hazards impose huge risks to the community as well as infrastructures. Obtaining and comprehending terrain features through geomorphological mapping is vital for dam area as it enables prediction of potential future terrain changes. The utilization of Unmanned Aerial Vehicles (UAVs) has garnered significant interest in geological, geomorphological, and geotechnical studies owing to their capacity to acquire high-resolution data from challenging structures like dams. This paper aims to assess the geomorphology characteristics such as topography of the embankment dam located at Bukit Kwong Dam, Kelantan Malaysia by utilizing the photogrammetric images acquired from UAV including Orthomosaic, Digital Surface Model (DSM) and points clouds using Structure from Motion (SfM) approach. An accuracy assessment for the generated DSM containing topography information was made to prove the reliability of the data. As a result, the millimetre uncertainty in the form of Root Mean Square Error (RMSE) was calculated approximately 8.04 mm and 0.33 mm for both horizontal and vertical accuracy respectively. The results demonstrate a high level of reliability to ensure the accuracy of future works such as hazards prediction in the dam area.

1 Introduction

Dam is a barrier that blocks or constrains the flow of water and raises the water level, forming a reservoir, lake, or an impoundment [1]. A created reservoir not only greatly suppress floods but also provide water for activities such as irrigation, human consumption, agriculture, and navigability and generation of hydropower [2,3]. At present, maintenance of large dams has become a contentious issue due to failure maintaining a regular assessment. Since 1970, Malaysia has also experienced number of dam incidences that had caused casualties to the downstream communities.

As stated by [4], four civilians were drowned due to flood at the spillway outlet of Sultan Abu Bakar Hydro Power Dam during monsoon season and the collapse of cofferdam due to overtopping at Peda Dam in 2012. These incidents should be taken seriously, and an effective

* Corresponding author: nasuhaishak21@gmail.com

dam safety assessment could have predicted and prevented most dam incidents progressing to dam failures. Hazards predictions and analysis usually requires an extensive source of data parameters that includes environmental, human engineering activities, geological and geomorphology in the area of interest [5]. Among all parameters, the geomorphology data that usually provides topography information is considered as the most crucial parameter in forming a basis for various hazard modelling such as flood inundation modelling, landslide susceptibility mapping and wildfire spread simulations [1]. The accuracy of these models relies on well updated topography and accurate elevation data to predict extent and severity of hazards [2].

In the past few years, digital photogrammetry based on Unmanned Aerial Vehicles (UAV) or known as drone is an irruptive technology that is being applied to many fields and industries such as mining, surveying, agricultures, environmental monitoring, and construction and infrastructures [6]. The utilization of UAV is especially ideal as it can easily and safely guided near high relief region and difficult situated structure like dams. From the UAV aerial images, various photogrammetric outputs can be derived such as orthophoto, points clouds and Digital Surface Model (DSM) [7]. Digital Surface Model (DSM) is a representation of the Earth's surface that includes natural terrain features such as mountains, valleys, and bodies of water, as well as anthropogenic features like buildings and infrastructure [6]. It can provide accurate detailed visual representation of the terrain which allow precise topography calculation of such as height, slope, aspect and terrain relief for hazard mapping, risk assessment and emergency preparedness strategies [6]. This study aims to obtain photogrammetric products derive from UAV technique to provide a groundwork as an accurate input data for further hazards prediction in dam area. This work is expected to provide essential spatial context to researchers to understand, predict and mitigate hazards more effectively.

2 Study area

The study area is located at Bukit Kwong dam with a catchment area of 11 square meter (m^2) and has a storage capacity of 14.3 million cubic metres at 16.76 meter Mean Sea Level (MSL), approximately eight kilometers southwest of Rantau Panjang in Pasir Mas district, Kelantan (Figure 1). It is an ageing embankment dam consisting of a turfed rip-rap stone and earthfill and was fully in operation since 1979. Bukit Kwong dam comprises of three main structures including main dam, gated service semi-circular spillway and irrigation intake headwork with the crest level of the dam is at 18.29 meter MSL. The dam region experiences a warm and temperate climate with seasonal monsoon climate and has been classified as an intermediate size dam with high hazard potential based on the International Commission on Large Dams (ICOLD) classification criteria.

Furthermore, there are an illegal deforestation activity nearby the reservoir area and the dam has once experienced a seepage incident at the downstream during monsoon season. Considering there is a high influence of uncertainty parameters in this region due to climate and illegal activities, this dam has been selected as a study area to possibly detect a potential landslide hazard for safety evolution and risk control.

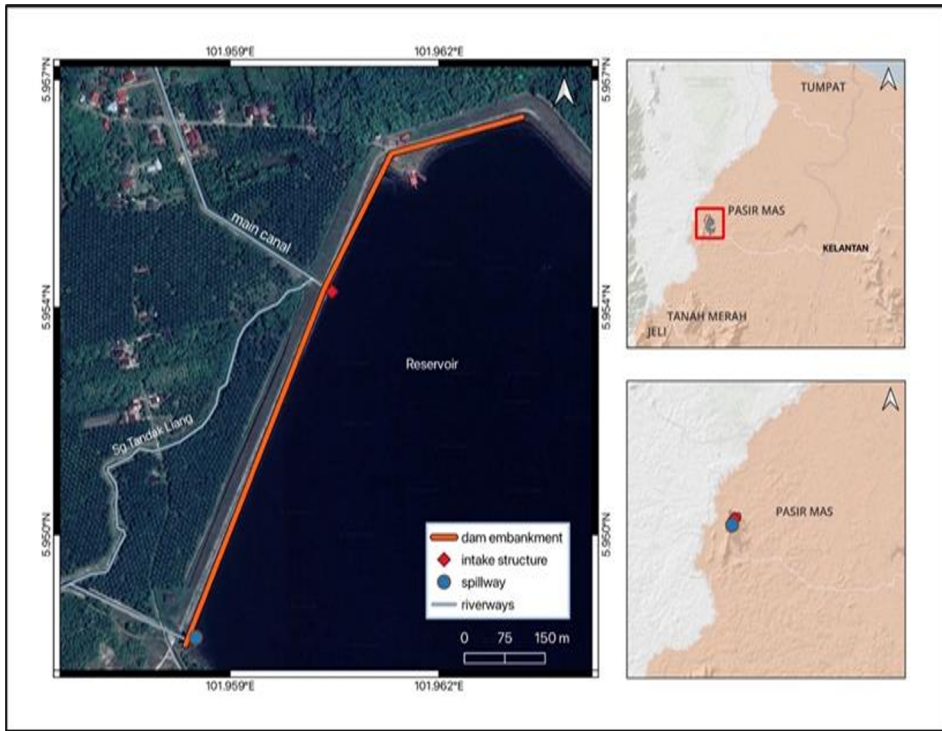


Figure 1. Location of Bukit Kwong Dam.

3 Methodology

3.1 Equipment

A rotary wing type of UAV with an integrated RGB (Red, Green and Blue) sensor, DJI Mavic 2 Pro (Figure 2) was used as a data image collector surrounding the dam area. This type of UAV has an advantage of being able to hover, take-off and land vertically besides of having better manoeuvring capability to get as close to the dam structure compared to a fixed wing UAV. The technical specification is shown as Table 1.



Figure 2. DJI Mavic 2 Pro.

Table 1. The technical specifications of DJI Mavic 2 Pro.

DJI Mavic 2 Pro Feature		Specifications
Aircraft	Dimension (mm)	322×242×84 (length×width×length)
	Weight (Inc. battery)	907 g
	Sensor	1" Complementary Metal-Oxide Semiconductor (CMOS)
Camera	Resolution	20 megapixels
	Focal Length (mm)	10.26
	Pixel size	2.4 × 2.4 μm
	Image Size	5472 × 3648
File format		jpeg / dng (raw)

3.2 Research methodology

There are five main phases involved to achieve the objectives of the study including (1) Literature review, (2) Data preparation and Planning, (3) Data Collection and Processing, (4) Results and Interpretation and (5) Accuracy Assessment as per illustrated in Figure 3.

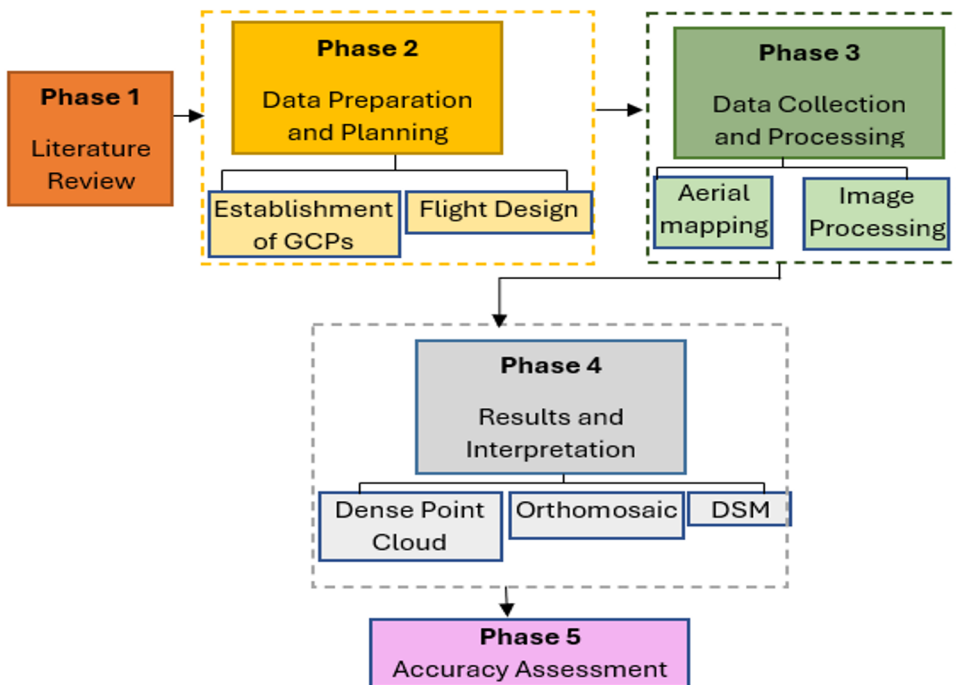


Figure 3. Flowchart of research methodology.

3.2.1 Literature review

The first phase of this study covers the literature review on the topic that includes types of UAV, UAV system, flight path, Ground Control Points (GCP), data processing, types of dam hazards and accuracy assessment.

3.2.2 Data preparation and planning.

During site and flight preparation, two vital processes were performed such as flight design and establishment of GCPs.

3.2.2.1 Flight design

The routes of the UAV were planned by ensuring the area of interest aligned within four coordinates, $5^{\circ}57'30.10''\text{N}$ $101^{\circ}57'30.61''\text{E}$, $5^{\circ}57'22.09''\text{N}$ $101^{\circ}57'57.89''\text{E}$, $5^{\circ}56'42.67''\text{N}$ $101^{\circ}57'41.85''\text{E}$, and $5^{\circ}56'51.79''\text{N}$ $101^{\circ}57'16.56''\text{E}$ as shown in Figure 4 (a) and (b). The area is free from power transmission line to avoid interference of signal with the photogrammetric configuration of 90% overlap and 85% side lap. All permits were obtained for site entry permission by Department of Irrigation and Drainage DID Kelantan State Director as well as Civil Aviation of Malaysia CAAM for flight permission. The boundary flight path of the study area was drawn in Google Earth using polygon shape and was imported to the DJI Go 4 app in an iPad that was connected via the cable to the remote controller.



Figure 4. Flight design of UAV survey. (a) Flight boundary and (b) parallel-axis flight lines of Bukit Kwong dam for UAV operation that includes dam, downstream and upstream area. Boundary mission was constructed in Google Earth in KML format and exported into UAV.

3.2.2.2 Establishment of GCPs.

The accuracy, distribution, and number of GCP can greatly influence the accuracy of DEM derived by UAV in different types of terrain [8]. There was a total of seven (7) GCPs targets where two of GCPs were located on the embankment area and the rest were distributed at the downstream and upstream area before the UAV mapping. The GCPs were measured using static network with a South Galaxy G7 base and rover. The GPS base station was first set up and observed on a stable ground and free from large obstacles within the study area for over 30 minutes of observation and all the GCPs location was measured and recorded using handheld rover. The coordinates were collected in the form of Easting (X), Northing (Y), and Elevation (Z) of GCPs and were processed simultaneously by connecting the points to the base station during data processing using Topcon Tool software.

3.2.3 Data collection and processing.

Data collection is a very crucial stage to ensure a high-resolution data by acquisition and overlapping of high quality photographs from good points of view. It consists of two main steps including aerial mapping and image processing.

3.2.3.1 Aerial mapping.

The flight and image acquisition were executed autonomously according to predefined flight path as per Figure 4 (b). Seven GCP targets were placed accordingly and were observed using spot measurement system. The details of technical parameters are indicated in Table 2.

Table 2. Technical parameters of the UAV operations

UAV Type	Altitude (m)	Area (kilometer ²)	Speed (m/s)	Duration	Total images
Multi-rotor	100	0.486	5.1	113 minutes and 33 seconds	2,297

3.2.3.2 Image processing.

The aerial images were processed using structure from-motion (SfM) technique via Agisoft software to create three-dimensional (3D) models from overlapping two-dimensional images. This technique produces a dense point cloud by automatically matching thousands of features (“tie-points”) in the multiple overlapping of 2D drone images [9]. The dense point cloud produced by this technique is comparable to LiDAR with the advantageous of lower cost, automation and ease of use [10]. The coordinate system for the outputs were set to Kertau 1968 / Kelantan Grid (EGM 96 Geoid).

3.2.4 Results and interpretation.

Three types of output were generated after the image processing steps including orthophoto, dense point clouds and Digital Surface Model (DSM). These outputs especially DSM is essential to give an early information about the terrain surface of the study area and serve as a basis in further analysis including risk assessment and hazards modelling.

3.2.5 Accuracy assessment.

The accuracy of the DSM was evaluated quantitatively using Root Mean Square Error (RMSE). According to [10], the formula for RMSE of difference between computed DSM and the initial position in X, Y, Z direction is given by Equations. 1-6 follows:

$$\left. \begin{aligned} \Delta X &= X_{\text{DSM}} - X_{\text{GCP}}; \Delta Y = Y_{\text{DSM}} - Y_{\text{GCP}} \\ \Delta Z &= Z_{\text{DSM}} - Z_{\text{GCP}}; \Delta XY = XY_{\text{DSM}} - XY_{\text{GCP}} \\ \Delta XYZ &= XYZ_{\text{DSM}} - XYZ_{\text{GCP}} \end{aligned} \right\} 1)$$

$$\text{RMSE}_X = \text{SQRT} \left[\left(\frac{1}{n} \right) \sum_{i=1}^n (X_{\text{DSM}} - X_{\text{GCP}i})^2 \right] \quad (2)$$

$$\text{RMSE}_Y = \text{SQRT} \left[\left(\frac{1}{n} \right) \sum_{i=1}^n (Y_{\text{DSM}} - Y_{\text{GCP}i})^2 \right] \quad (3)$$

$$\text{RMSE}_{XY} = \text{SQRT} \left[(1/n) \sum_{i=1}^n (\Delta X)^2 + (\Delta Y)^2 \right] \quad (4)$$

$$\text{RMSE}_Z = \text{SQRT} \left[(1/n) \sum_{i=1}^n (\Delta Z)^2 \right] \quad (5)$$

$$\text{RMSE}_{XYZ} = \text{SQRT} \left[\left(\frac{1}{n} \right) \sum_{i=1}^n ((\Delta X)^2 + (\Delta Y)^2 + (\Delta Z)^2) \right] \quad (6)$$

where,

$X_{\text{GCP}i}$ and X_{DSM} are the X-coordinate component of GCP and corresponding coordinate in DSM, respectively;

$Y_{\text{GCP}i}$ and Y_{DSM} are the Y-coordinate component of GCP and corresponding coordinate in DSM, respectively;

$Z_{\text{GCP}i}$ and Z_{DSM} are the Z-coordinate component of GCP and corresponding coordinate in DSM, respectively.

4 Result

To assess the quality of the overall results for this study, three main criteria were analysed including: (1) quality check assessment, (2) points clouds, orthomosaic and digital surface model, and (3) accuracy assessment.

4.1 Quality check assessment

The quality check was made to give an overview regarding the quality and accuracy of this study. Figure 5 shows the summary and quality check of the dataset and digital images used in this study. There were 2,043 out of 2,297 images were calibrated which is about 88% of the images. This is due to features of water that has caused an overlapping limitation at the reservoir. It can be seen from Figure 6 (a) and (b), the images at the reservoir have low overlap since the water features reflect light which causes glare and distorting the images and thus complicates the matching of the images [8]. The ground resolution or Ground Sampling Distance (GSD) was found relatively high with each pixel in image represent an area on the ground by approximately 2.34 centimetre. A smaller GSD means higher spatial resolution that is crucial for capturing detailed imagery, which is important for tasks like object detection, mapping, and analysis [8].

Number of images:	2,043	Camera stations:	2,035
Flying altitude:	104 m	Tie points:	949,513
Ground resolution:	2.34 cm/pix	Projections:	3,419,413
Coverage area:	0.45 km ²	Reprojection error:	3.91 pix

Camera Model	Resolution	Focal Length	Pixel Size	Precalibrated
Test_Pro (10.26mm)	5472 x 3648	10.26 mm	2.41 x 2.41 μm	No

Figure 5. The summary and quality check for quality assessment.

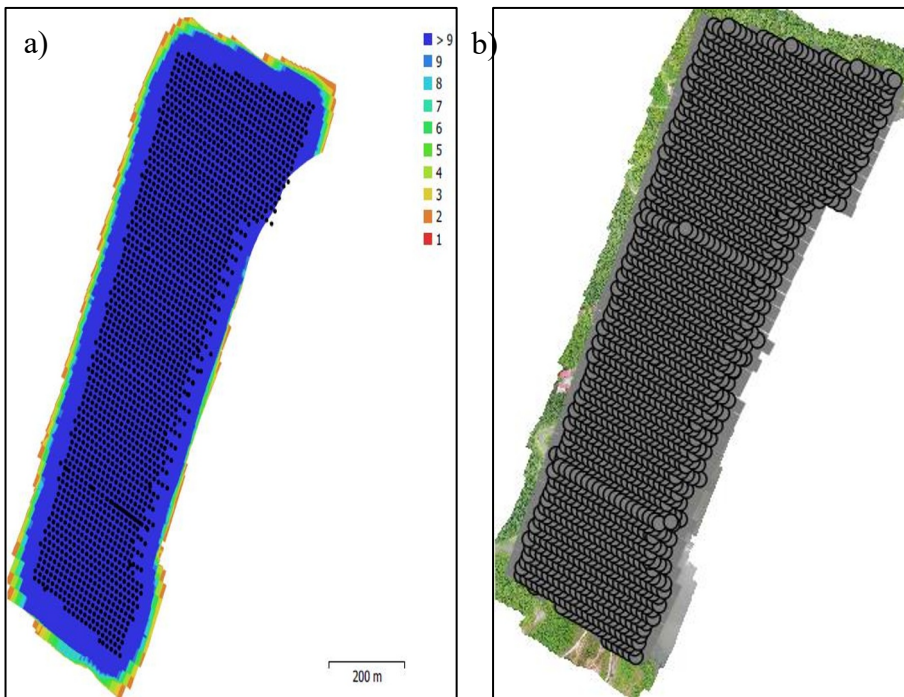


Figure 6. a) Number of overlapping images computed for each pixel. Red areas indicates low overlap images around the edges and reservoir area. (b) The links of computed image positions and matched 2D keypoints between images. Greyed out lines indicate weak links which were found at the reservoir area.

4.2 Point Clouds, orthomosaic and digital surface model

The density of the point clouds was attained a total of 55,771,275 points in the study area. The generated 3D point clouds (Figure 7 (a)) successfully covered various land cover types such as vegetations, drain, earth fill embankment, spillway, road, buildings, hills, and trees. It was noticed that the reservoir area had minimal points, however it was expected as the water features typically lack distinct features that were harder for object recognition. In general, these point clouds are considered high density, averaging approximately 114 points

per cubic meter. This contrasts with similar case studies, which average 70 points per cubic meter [11]. The spatial resolution of generated orthomosaic (Figure 7 (b)) was acquired approximately 2.34 centimetre and effectively reconstructed the study area with no visible angular distortions in a complex surface area such as river and dense forest cover. Similar to spatial resolution, the created digital surface model (DSM) (Figure 7 (c)) had classified the dense points clouds into several classes with the elevations ranging between 12.8 meter to 42.8 meter. These categorized land types are especially vital for hazard mapping and can be further used to extract their geomorphology information such as slope, aspect, curvature, and elevation.

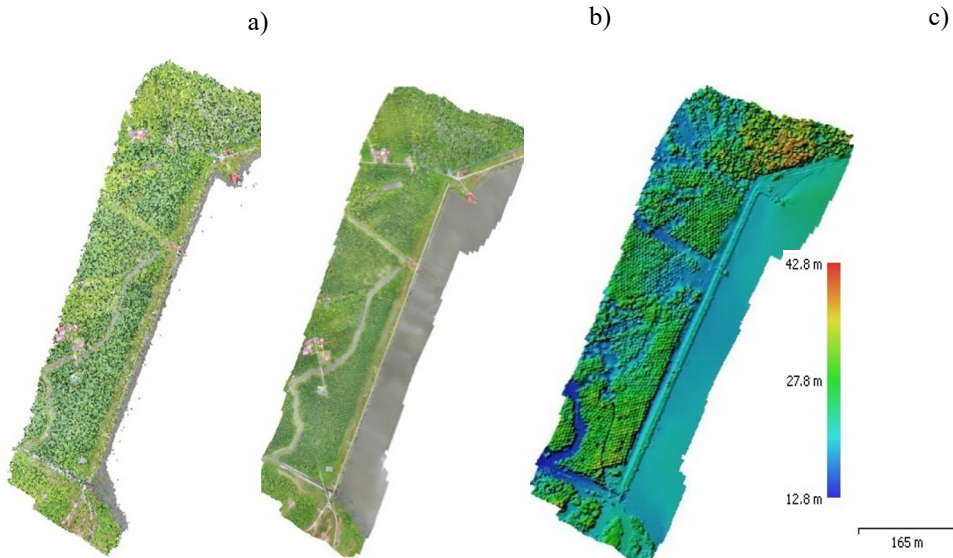


Figure 7. (a) Dense point clouds. (b) Orthomosaic showing the landscape of the study area. Some image distortions were found at the reservoir. (c) Digital surface model of the rockfill and earthfill embankment dam. The colour bar shows the surface elevation (in meters).

4.3 Accuracy assessment

Table 3 summarized the RMSE in three coordinates direction of X, Y and Z error for each distributed GCP (Figure 8) which were obtained in millimetre (mm) accuracy. The XYZ errors were seen extremely low errors values ranging from -12 mm to 7 mm. The RMSE value for horizontal error was calculated approximately 8.04 mm using the Equation 4 and the accuracy for vertical was approximately 0.33 mm. The data was seen exhibited a larger error along the horizontal axis than the vertical axis. In UAV photogrammetry, it is widely acknowledged that horizontal accuracy tends to be slightly superior to vertical accuracy, except in cases of complex topography such as hilly areas and sloped terrain [3]. An embankment dam is usually situated in a high relief area where typically has higher horizontal RMSE between $1 \times \text{GSD}$ to $7 \times \text{GSD}$ and a vertical RMSE between $1.5 \times \text{GSD}$ to $5 \times \text{GSD}$ as reported by various studies [12,13]. Generally, the quality of the produced DSM was found extremely better as compared to the study by [14] with the RMSE accuracy of 0.20 meter using a high GCP density (40 GCPs) distributed in a small survey area (0.2 km^2).



Figure 8. The distribution of seven ground control points in study area. Two GCPs (GCP 6 and 7) located at centre on embankment crest, while five GCPs located at upstream (GCP1, GCP 2), downstream (GCP 4 and 5) and at upper edge (GCP3) of study area.

Table 3. The root mean square error of ground control points

Label	X error (mm)	Y error (mm)	Z error (mm)	Total (mm)
GCP1	6.21798	0.380583	0.623949	6.26078
GCP2	-9.22091	0.755356	-0.24618	9.25507
GCP3	-12.3145	-4.26877	-0.0806107	13.0336
GCP4	0.886831	7.00287	-0.068844	7.05913
GCP5	3.24527	0.782354	0.250206	3.3476
GCP6	5.5132	-5.81008	-0.508289	8.02563
GCP7	5.6721	1.15768	0.0297716	5.78911
RMS error (mm)	7.0632	3.8487	0.334451	8.05066

5 Discussion

In this study, the quality of the DSM was validated using RMSE which has been repeatedly used in literature where the lower RMSE value indicated the model's reliability [15,16]. The results demonstrated the standard error of the seven GCPs for the whole study area was in total precision of approximately 8 mm. Based on Table 3, the highest height and spatial error of the GCPs indicate values of ± 0.6 mm and ± 12 mm for GCP 1 and GCP 3 respectively. Corresponding to these errors, the point cloud around both GCP 1 and GCP 3 were seen exhibited slightly sparse density on these regions as shown in Figure 9 (a) and (b), as the areas experienced the highest error.

Furthermore, GCP 1 was located near to the hilly terrain covered with dense canopy trees with height variations. This may have caused some adversity for the model to distinguish between top of canopy and ground level in complex terrains and thus lead to higher a vertical error [15]. In contrast in the area around GCP 7 with lower error, the embankment area can be seen fully reconstructed with dense point clouds (Figure 9 (c)) showing great details including the crest as well as the materials fills (rip-rap stone and earth fill). The precision of results are greatly varied with distribution of GCPs rather than different number of GCP for better accuracy in both vertical and horizontal accuracy [17]. In this study, millimeter accuracy was achieved which indicates sufficient and well distributed GCPs at the study area.

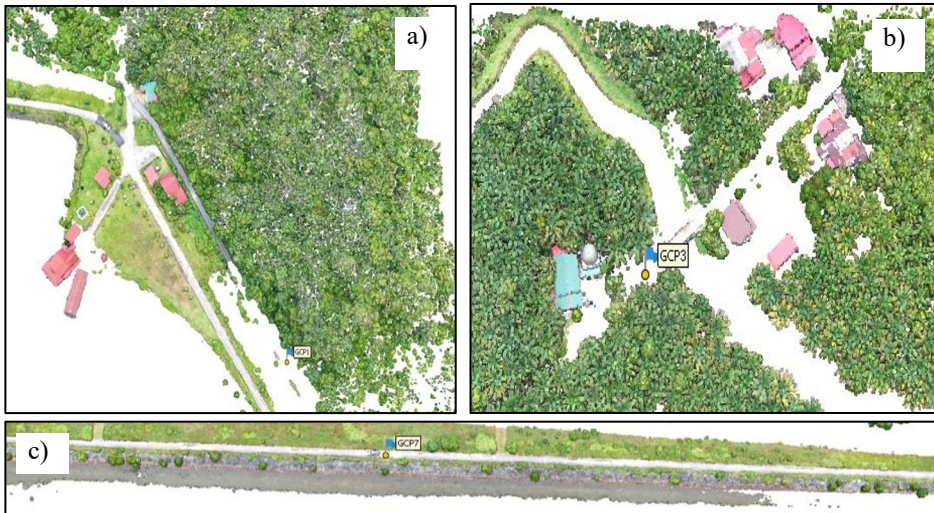


Figure 9. The density of point cloud at (a) GCP 1, (b) GCP 3, and(c) GCP 7

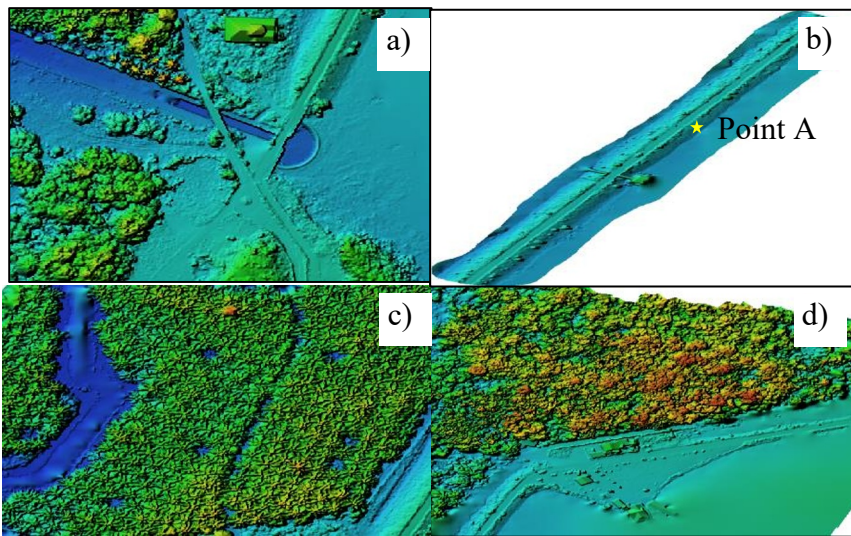


Figure 10. The geomorphology based on the reconstructed digital surface model of the study area a) flat and low dissected plateau, (b) moderate straight steep terrain. Point A was extracted to retrieve morphometric information, (c) flat valley with vegetation cover and (d) moderate dissected hills and valley.

The geomorphology of the study area were identified consisting of flat and low dissected plateau (Figure 10 (a)), flat valley with vegetation cover consisting of river (Figure 10 (c)), moderate dissected hills and valley (Figure 10 (d)) and moderate straight steep terrain across the reservoir (Figure 10 (b)). The morphological characteristics (i.e., slope, aspect, elevation) of Point A (Figure 10 (b)) at the embankment fill was selected randomly and extracted from the DSM using ArcGIS software to represent and highlight the features of the area. As shown in Table 4, the slope angle at the Point A is 15 degree in the direction of northeast with moderately high altitude at 24.8 meter. In an embankment dam, slope angle of 15 degree could become critical if the factors like water saturation or poor soil cohesion are involved [16]. Moreover, if the direction of the slopes are facing with an extreme precipitation possibly leading to a higher moisture retention and thus susceptible to saturation and potential instability especially at higher elevations [15]. According to [17], the surface landform features such as slope angle, aspect and elevation are crucial as primary data in the study of slope instability and movement of soil mass or landslide. In addition, layering multiple parameters of various resources (e.g. lithology, rainfall, soil), a significant instability events can be defined in the study area liable to comparatively high or else low probability or probability classes [16].

Table 4. Morphometric features of Point A at the embankment fill area

	Slope (Degree)	Aspect	Elevation (meter)
Embankment Fill Area	15	Northeast	24.8

6 Conclusion and recommendations

This study examine the feasibility of using UAV technique to acquire high quality and accurate geomorphology information and model for further possible hazard mapping and assesment. The DJI Mavic 2 Pro was equipped with RGB sensor and was flown 100 meter above the ground surface with overlap 90%, and 85% along and across track respectively. A total of 2,043 images were used and produced spatial résolutions of 2.34 centimetre for both generated orthomosaic and DSM. Both outputs gave visibly competent results with great details and no angular distorsion especially in complex surface such as dense vegetation and river. However, the water features in the reservoir area was unable tu fully reconstructed due to lack of distinguished oboject. It is advisable for similar work to use polarizing filters or manually tie key points to improve the mapping over the water features. The dense point cloud was acquired almost sixty million and well distributed in a challenging features such as dense canopy of trees as well as the dam embankment crest. The number and distribution of 7-GCPs were found adequate and well distributed across the study area. The geomorphology and morphometric features were succesfully defined with great vertical and horizontal RMSEs accuracy of 8.04 mm and 0.33 mm accuracy respectively. In view of these results, great reliability and sufficiency is expected for future work such as hazard assesment and prediction for the embankment dam.

References

1. M. Chang, C. Luo, B. Wu, L. Xiang, J. Hydrol, **609**, 127729 (2022)
2. E.M Latrubesse, E. Park, K. Sieh, T. Dang, Y.N. Lin, S.H. Yun, *Geomorphology* **362** 107221 (2020)
3. R. Xiao, M. Jiang, Z. Li, X. He, *Int J Appl Earth Obs Geoinf*, **107**, 102705 (2022)
4. Malaysia Dam Safety Management Guidelines (MyDAMS) (Kuala Lumpur: Jabatan

- Pengairan dan Saliran Malaysia) ISBN 978-983-41328-5-9 (2017)
5. T. Mersha, M. Meten, *Geoenvironmental disasters* **7** 1-22 (2020)
 6. M. Błaszczyk, M. Laska, A. Sivertsen, S.D. Jawak, *Remote Sens (Basel)*, **14**(3) 601. (2022)
 7. P. Han, C. Ma, J. Chen, L. Chen, S. Bu, S Xu, T. Hagino, *Remote Sens (Basel)*, **14**(16) 4113 (2022)
 8. E. Sanz-Ablanedo, J.H. Chandler, P. Ballesteros-Pérez, J.R. Rodríguez-Pérez, *Earth Surf Process Landf* **45**(9) 2134-2147 (2020)
 9. J.I. Shin, Y.M. Cho, P.C. Lim, H.M. Lee, H.Y. Ahn, C.W. Park, T. Kim, *Remote Sens (Basel)*, **12**(11) 1726 (2020)
 10. T. Khuc, T.A. Nguyen, H. Dao, F.N. Catbas, *Measurement* **159**, 107769, (2020)
 11. C. Wang, I. Sasanakul, H. Brown, *GI_Forum* **202**, 9 5-12 (2021)
 12. F. Agüera-Vega, F. Carvajal-Ramirez, P. Martínez-Carricondo, J.S.H. López, F.J. Mesas-Carrascosa, A. García-Ferrer, F.J. Pérez-Porras, *Measurement* **121**, 127-138 (2018)
 13. S.I. Jiménez-Jiménez, W. Ojeda-Bustamante, M.D.J. Marcial-Pablo, J. Enciso, *ISPRS Int J Geoinf* **10**(5) 285 (2021)
 14. A.R. Groos, R. Aeschbacher, M. Fischer, N. Kohler, C. Mayer, A. Senn-Rist, *Front. remote sens* **3**, 871994 (2022)
 15. R.M. Yuvaraj, B. Dolui, *Environ Chall (Amst)* **5**, 100211 (2021)
 16. M.K.T.M. Yusof, A.S.A. Rashid, M.F.A. Khanan, M.Z.A. Rahman, W.A.A. Manan, R. Kalatehjari, A. Dehghanbanadaki, *Phys Chem Earth (2002), Parts A/B/C* **133**, 103496 (2024)
 17. I. Sonker, J.N. Tripathi, Swarnim, *Nat Hazards*, **120**(7), 6797-6832 (2024)